Specialized methods for direct numerical simulations in porous media

Sven Linden, Liping Cheng, Andreas Wiegmann

Math2Market GmbH, Kaiserslautern, Germany

Summary:

3D imaging methods, such as micro computed tomography or focused ion beam scanning electron microscopy, allow deep insights into the three-dimensional structure of porous materials. The resulting 3D data sets are very large, often exceeding 2000^3 or 8 billion volume elements called voxels. Researchers and engineers are interested in determining effective homogenized material properties based on these data sets to understand existing materials or to design new man-made materials. Recent advances in software technologies have made it possible to compute and visualize effective properties such as permeability, and thermal or electrical conductivity on these large images in very short times and using surprisingly little memory.

Classical finite-element or finite-volume methods are not suited to compute physical properties on these large images. The bottleneck of these methods is the mesh generation that must be done before the actual simulation can take place and can take longer than the solving of the discretized partial differential equation. Instead, complex microstructures are best dealt with by fast and memory efficient numerical methods that are explicitly designed for them.

In this paper, we present state-of-the-art numerical finite-volume-based and fast Fourier transformation-based methods which do not require mesh generation and are designed to compute effective properties directly on very large 3D images. We also present relevant application areas where these methods are used successfully and how simulations on the microscale help to encourage computational material research and development.

Keywords:

Direct Numerical Simulation, Finite-Volume, Fast Fourier Transformation, Pore Morphology, Lippmann Schwinger

1 Introduction

3D imaging methods and devices developed during the last decades allow a penetrating look inside natural and man-made materials. Especially micro computed tomography (µCT) scanning devices with voxel lengths down to 250 nm and focused ion beam scanning electron microscopy (FIB-SEM) with voxel lengths down to 10 nm allow insights into the three-dimensional structure of porous materials. Nowadays, 3D images with 2000^3 (or 8 billion) voxels are a standard size that can be imaged and reconstructed within hours.

With the development of 64-Bit technology and increase in computational power, it became possible to visualize and compute effective properties on these large 3D images. But very fast and memory efficient numerical methods are needed. Many researchers and engineers are interested in effective homogenized material properties such as

- permeability, pressure drop and mean velocity,
- thermal and electrical conductivity,
- diffusivity and tortuosity,
- stiffness, strain, stress, or elastic moduli,
- saturation- or compression-dependent properties such as relative permeability.

Classical finite-element or finite-volume methods are not suited to compute physical properties on these large images. The bottleneck of these methods is the mesh generation that must be done before the actual simulation can take place. In many cases, simulation engineers must adjust the generated meshes manually to ensure that simulations converge properly and provide the desired accuracy. In addition, mesh generation often takes more runtime than the actual solving of the discretized partial differential equations (PDE).

For computation of flow properties, Lattice-Boltzmann (LB) methods which do not require mesh generation [1] are used by many researchers. For computation of conductive/diffusive and mechanical properties, methods that make use of the fast Fourier transformation (FFT) are advancing fast [2]. Both LB and FFT methods work on the voxel grid directly without any meshing.

Our group at Math2Market also makes use of these methods but years ago decided not to develop our LB methods any further and instead focus on finite-volume and FFT-based methods. The LB methods have the disadvantage of requiring more memory due to the D3Qm lattices. On the other hand, finite-volume-base and FFT-based methods can be discretized in such a way that they work on voxel grids just on the original variables of the PDE. Thus, they require less memory than LB methods. In addition, the development of adaptive grid methods made it possible to additionally reduce the memory usage. The combination of geometric two-phase methods and single-phase finite-volume methods also allows to compute saturation-dependent properties such as relative permeability.

In this paper, we give an overview of our state-of-the-art finite-volume and FFT-based methods. In addition, we present significant application areas where these methods are used successfully and how simulations on the microscale help to incite material research and development.

2 Direct numerical methods

GeoDict, the digital material laboratory software developed by Math2Market GmbH, brings five different solution methods into play for the simulation of single-phase and two-phase fluid flow, conduction, and mechanics in porous media. First, we start with the single-phase fluid flow solvers. The solvers are in order of their inception: Explicit Jump (EJ-Stokes), SIMPLE-FFT, and LIR. The common denominator of all three solvers are (1) the direct simulation on 3D images (e.g. µCT scans), (2) their usage of a finite volume formulation, and (3) their discretization of the no-slip boundary conditions. The EJ and LIR methods can also be used for the simulation of conductivity, i.e. solving the Poisson equation.

2.1 The Explicit Jump formulation for Flow and Conduction Simulation.

In 1965, Harlow and Welch [3], introduced a finite volume formulation on a staggered grid. Simplifying this formulation for voxels (the little cubes a digital 3D image is thought to be made of), it can be said that the pressure variables represent an average for the whole cube and live at the cube centers, whereas the velocities represent transport across faces between the cubes and live on the respective faces of the cube. That is, the x-velocity lives on the left and right x-faces of the cube, the y-velocity lives on front and back faces of the cube, and the z- velocity lives on the bottom and top faces of the cube.

A predecessor of EJ-Stokes, the FFF-Stokes method by Wiegmann in 2007 [4], used this staggered grid formulation, but implemented the no-slip boundary conditions with less accuracy than originally suggested by Harlow and Welch, and was based on ideas by Wiegmann and Bube in 2000 [5]. The steady-state Stokes equations for laminar flows is described by

$$\begin{aligned} \mu\Delta u - \nabla p &= f && \text{momentum conservation} \\ \nabla \cdot u &= 0 && \text{mass conservation} \\ u|_{\partial\Omega} &= 0 && \text{no-slip boundary condition} \end{aligned} \qquad (1)$$

with constant viscosity μ, velocity u and pressure p in the domain Ω. The domain is periodic and the direction of the flow is induced by the unit vector f that always points in the direction of one of the coordinate axes. The Stokes operator is decoupled into four Poisson problems, and each Poisson problem is solved by a Fast Fourier Transform (FFT) approach. The details of FFT-based fast Poisson solvers can be found in Swarztrauber [6]. The Poisson problem approach is at the base of the speed of the FFF-Stokes, EJ-Stokes, and SIMPLE-FFT solvers. These solvers are made explicitly to work on 3d images, which have the regular grid spacing needed to use the FFT and are the main reason for the FFT's high performance.

The FFF-Stokes solver over-simplified the discretization of the no-slip boundary conditions at the price of reduced accuracy for pores in the shape of narrow channels. EJ-Stokes overcomes this limitation by implementing the original boundary conditions from Harlow & Welch (see also Fig.1), i.e. has higher accuracy. EJ-Stokes uses the Biconjugate gradient stabilized method [7] to solve the derived non-symmetric linear system of equations. A Schur-complement for auxiliary (Explicit-Jump) variables represents discontinuities in the flow velocity derivatives and is iterated until the residual has reached a small enough value or until the derived permeability has converged sufficiently well.

The natural boundary conditions for the EJ-Stokes solver are periodic boundary conditions for the flow variables on all six faces of the 3d image and no-slip boundary conditions on the solid surfaces. Due to the staggered grid, no boundary conditions are needed for the pressure variables at the no-slip solid surfaces, periodic boundary conditions are used on the four tangential faces and, in the direction of the flow, a discontinuity in the pressure of the magnitude of the specified pressure drop is implemented. Symmetry conditions in the tangential direction and constant pressures on inlet and outlet can be enforced by appropriate mirroring of the computational domain.

As mentioned before, the EJ-Stokes solver is specifically made for computations on 3D and 2D images, such as segmented CT scans and segmented FIB-SEM scans. A drawback is that the solver allocates memory also for the solid portions of the image and not only for the pore space. It also converges slowly for low porosity structures with high geometric complexity compared to high porosity structures with low geometric complexity. The EJ-Stokes approach does not (yet) extend to the Stokes-Brinkman, Navier-Stokes, and Navier-Stokes-Brinkman equations. A strong point is that it typically requires less than 10% of the memory needed by a Lattice-Boltzmann implementation on the same image while converging significantly faster for the same image and same accuracy. The Explicit Jump formalism also allows to solve the:

$$\nabla \cdot (\beta \nabla U) = f \qquad \text{Poisson equation} \qquad (2)$$

with isotropic conductivity β and scalar temperature (or electric potential) U. Here, harmonic averaging is used to compute conductivities at voxel faces and explicit jump variables across material interfaces are introduced to represent discontinuities of temperature derivatives. Again, a Schur-complement formulation for the jump variables is derived and solved by using the FFT and BiCGStab methods [8]. The convergence speed of this method is almost independent of the conductivity contrast which is a very big advantage compared to other approaches.

2.2 SimpleFFT for Flow Simulations

SIMPLE-FFT is a variant, and FFT-accelerated version, of the Semi-Implicit Method for Pressure-Linked Equations, or SIMPLE [9] algorithm. SIMPLE-FFT is a finite-volume method on a staggered grid. With the classic SIMPLE algorithm, the flow field is firstly approximated by solving the momentum equation, in which the pressure gradient term is set from an initial guess or calculated using the pressure distribution from the previous iteration. The pressure correction equation is formulated and solved to obtain a new pressure distribution. Velocities are then corrected. The iterations continue until they reach a certain stopping criterion.

For porous media, due to their complex connectivity, the classical SIMPLE algorithm has difficulty converging to the solution of the steady state Stokes equations. Solving the pressure correction equation was identified as the bottleneck of convergence because the inaccuracy of the pressure correction step requires excessively many iterations. In SIMPLE-FFT, the FFT is then used to solve the pressure correction Poisson equation exactly instead of just taking a single step. This reduces the iterations and computation times dramatically even though the cost of an individual iteration rises significantly.

With no-slip boundary condition on the wall, as shown in Fig. 1, the velocity components $u_{i,j+1}$, $u_{i,j}$, and $u_{i,j-1}$ are the surface variables on the true wall surfaces in the normal direction of a solid, so they are all zero. In the tangential direction, because the surface variables are half mesh size off the computation

variables, following Harlow and Welsh two cells neighboring to the interface must be considered: one in the solid and the other in the void domain. We set $v_{i,j} = -v_{i,j-1}$ to get the first order approximation of zero velocity on the wall.

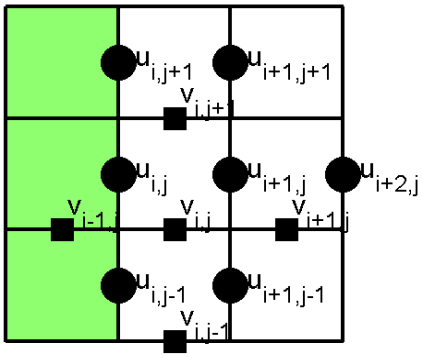

Fig. 1: shows a 2D example with the surface variables in the horizontal (circles) and vertical directions (squares).

When there exists unresolved porosity in the structure, i.e., some of the voxels are permeable, the Stokes-Brinkman equations can be solved with SIMPLE-FFT by providing the permeability of the porous voxels. When the flow is fast and Darcy's law does not hold any more, SIMPLE-FFT solves Navier-Stokes equations, and when both fast flow and porous voxels are present, Navier-Stokes-Brinkman equations are solved.
SIMPLE-FFT runs on the uniform Cartesian grid of a 3D image and, on each grid cell, three velocity components and pressure need to be found. The variables inside the solid are enforced to zero. SIMPLE-FFT has its advantages when a structure has low porosity while only the unknown variables in the void spaces are to be solved and the pressure correction can be propagated to the velocity correction quickly. Fewer iterations and lower runtime are required compared to structures with the same size but higher porosity. On the other hand, when the porosity of a structure is higher, there are more unknowns and the momentum equations still need a high number of iterations to solve the velocity field even though the pressure correction can be easily found with the FFT algorithm. The memory usage of SIMPLE-FFT is decided by the grid size, regardless of the porosity. SIMPLE-FFT requires more memory when compared to the EJ and LIR solvers.

2.3 LIR for Flow and Conduction Simulations

The LIR [10] is the newest, a very fast and memory efficient iterative finite volume method. The solver computes the permeability, as well as velocity and pressure fields, on large 3D images. As happens for the SIMPLE-FFT, the LIR solver can be used for the numerical solution of the Stokes, Stokes-Brinkman, Navier-Stokes, and Navier-Stokes-Brinkman equations.
Usually, 3D images are represented as regular voxel grids where the number of grid cells grows cubically. The LIR solver uses an adaptive grid, instead of a regular grid, to reduce significantly the number of grid cells. The basis of the adaptive grid is a data structure called LIR-tree (a combination of Octree and KD-tree) that is used for spatial partitioning of 3D images [11]. The pores are represented as differently sized rectangular cuboid cells. Solid regions do not require any computational memory. The pore space is coarsened in areas with small velocity and pressure variations, while keeping the original resolution near the solid surfaces and in regions where velocity or pressure vary rapidly.
Variables are arranged in such a way that each cell can satisfy the (Navier-)Stokes(-Brinkman)-equations independently from its neighbor cells. Pressure and velocity are discretized on staggered grids (see also Fig. 1) but two velocity variables, namely one for each neighboring cell, are introduced instead of using one velocity variable on the cell faces. The two velocity variables discretize the two one-sided limits at the center of the cell surface. The discretization of the momentum and mass conservation equations yields one 7x7 linear system (block) per cell. This block structure allows using the block Gauß-Seidel algorithm as an iterative solver method. The advantage of that approach is that the Stokes equations can be solved directly without using a pressure correction equation, as happens in many other approaches (e.g. SIMPLE).
The LIR solver is very fast and very memory efficient for highly porous structures. For low porosity structures, the solver needs more iterations until the desired accuracy is reached than for highly porous structures. Here, the convergence speed depends on the complexity and inhomogeneity of the pore space. The runtime per iteration is very low due to the small number of cells. Thus, the solver is also fast and very memory efficient for low porosity structures. The convergence of the solver can be increased significantly by two methods:

- Successive Over-Relaxation (SOR) instead of Gauß-Seidel algorithm
- Multigrid methods which make use of coarser grids to reduce low-frequency residuals

Limitations of that approach are the modelling of very fast flows with high Reynolds numbers and emerging turbulence and boundary layers. Moreover, modelling of slip-boundary conditions is also very difficult. However, these limitations apply to all methods that use voxel grids.
Similar to the EJ formalism, the LIR formalism also allows to solve the Poisson equation (stationary heat equation). Conductivities at cell faces are computed by harmonic averaging of conductivities. Here, temperature (or electric potential) live at the cell center and two flux variables discretize the two one-sided limits at the center of the cell surface.

2.4 Lippmann Schwinger for Mechanics Simulations

In the previous sections, we discussed three different approaches to solve the (Navier-)Stokes(-Brinkman) equations. Two of them can also be used to solve conduction equations. In this section, we present the basic idea of a method that is used for linear and non-linear structural mechanics simulations.
For a uniform macroscopic strain S, we solve the boundary value problem (BVP):

$$\begin{aligned} \nabla \cdot \sigma &= 0 && \text{Equilibrium of stress} \\ \sigma &= C : \epsilon && \text{Hooke's law} \\ 2\epsilon &= 2S + \nabla u^* + (\nabla u^*)^T \end{aligned} \qquad (3)$$

for the stress field σ, strain field ϵ, and the displacement field u^*. The BVP or equations of linear elasticity consists of the elastic equilibrium equation, Hooke's law, and periodic boundary conditions. By introducing a reference material of homogeneous stiffness C_0, the BVP can be transformed into the strain-based Lippmann-Schwinger equation, implemented in the FeelMath Solver

$$(I + B_\epsilon)\epsilon = \epsilon + \Gamma_0 * \big((C - C_0) : \epsilon\big) = E \qquad \text{Lippmann-Schwinger equation} \qquad (4)$$

Fast Fourier transforms allows to solve the convolution with the Green's operator Γ_0 [12]. The Lippmann-Schwinger equation can also be formulated with respect of stress instead of strain. These equations can iteratively be solved using the Neumann series expansion, the so-called basis scheme. Instead of using the Neumann series expansion, Krylov subspace methods can be applied to accelerate the convergence of the method but requiring more memory. The formulation allows to handle linear and non-linear (i.e. replacing Hooke's law with a non-linear formulation) material laws as well as isotropic, transverse-isotropic, orthotropic, or anisotropic constituent materials.
Similar to the flow solvers, a staggered grid is used to discretize displacement, strain, and stress variables [13]. That is, the x-displacements live on x-faces, the y-displacements live on y-faces, and the z-displacements lives on the z-faces of the voxels. The diagonal entries of the strain and stress tensors live on the voxel center, the xy-entries live on the center of the z-edges, the yz-entries live on the center of the x-edges, and the xz-entries live on the center of the y-edges of the voxels.
The number of iterations that is required until convergence of the stiffness depends on the largest phase contrast ρ in the structure and the solution scheme. If the basic scheme with Neumann series approximation is used, then the number of iterations grows linearly with ρ. For accelerated schemes where Krylov subspace methods are used, the number of iterations grows with $\sqrt{\rho}$.
For the computation of compression dependent properties, the displacement field u^* used to predict a compressed structure. The voxels of the original image are moved along the displacement field and cut with a reduced voxel image. The result of that procedure is a gray-value image where a global threshold is used to perform a segmentation of the different phases. The threshold is chosen in FeelMath such that either mass or volume is preserved.

2.5 Pore Morphology methods for Two-Phase Flow Simulations

The EJ, SIMPLE-FFT, and LIR methods solve the discretized single-phase (Navier-)Stokes(-Brinkman) equations. As post-processing step, the methods yield the absolute permeability of porous media. However, in many application areas, researchers are interested in saturation-depended properties such as relative permeability. For relative permeability, we must solve two-phase flow equations instead of single-phase flow equations. In these flow regimes, capillary forces caused by surface tension and capillary pressure are often dominating compared to viscous forces, i.e. capillary number is low. The solution of these two-phase flow equations is very challenging, and runtimes are very high. Here, we present an alternative approach.
The pore morphology method [14], also known as maximum inscribed spheres [15], predicts the distribution of a wetting phase (WP) and a non-wetting phase (NWP) inside a porous medium. The

method distributes two fluids by using morphological operations rather than solving partial differential equations. There are two possible scenarios:

- Drainage: the WP is drained from the structure and gets displaced by the NWP
- Imbibition: the WP imbibes the structure and displaces the NWP.

For drainage, it can be envisioned that spheres are pushed into the structure and placed in the pore space where the pore size is greater than a certain radius. The radius is decreased in an iterative process and this corresponds to an increase of the capillary pressure. The superposition of all spheres represents the NWP. The pore morphology method achieves this placement of spheres by dilation and erosion processes of the solid phase with the pore space. Additional connectivity checks [16] with respect to NWP and WP reservoirs can be used to increase the validity of the distributions. These connectivity checks allow the algorithm to introduce residual phases where parts of the NWP are trapped and cannot leave the simulated domain.
The output of the algorithm is a finite sequence of quasi-stationary states. Each state is a 3D image again that encodes the solid phase, WP, and NWP. As post-processing, the Young-Laplace equation based on the radii of the inscribed spheres and the interfacial tension predicts the capillary pressure

$$p_c = 2\frac{\gamma}{r}cos\alpha \qquad \text{Young-Laplace equation} \qquad (5)$$

with capillary pressure p_c, surface tension γ, pore radius r, and contact angle α. The method was extended by Schulz et al. [17] to handle multiple contact angles within the same structure. This can be achieved by using different radii for the dilation process but a single radius for the erosion process. It is also possible to simulate hysteresis processes where drainage and imbibition happen in series. The highest capillary pressure that can be simulated depends on the voxel length of the structure. One of the current limitations of these methods is that mixed wettability cannot be simulated. Mixed wettability means that a fluid is wetting on one material and non-wetting on another material within the same simulated domain.
The computation of relative permeability is done with the sequence of quasi-stationary states. For relative permeability of the WP, for instance, we solve a single-phase flow inside the WP and treat the interface between WP and NWP as immobile no-slip interface.

3 Application examples

In this section, we present application areas and refer to literature where the above methods have been used. Each application area involves distinct media and exhibits different numerical challenges.

3.1 Filtration

Filters are essential in industry and in everyday life, to preserve machine functionality and for protection against toxic and allergenic substances. The demands on filter efficiency, selectivity, capacity, and filter lifetime increase constantly and highly specialized solutions are needed for every filtration application. Simulations help filter media makers and filter manufacturers understand and productively improve existing filter materials. Important filter characteristics are:

- initial pressure drop: pressure drop between inlet and outlet of a clean filter,
- filter efficiency: quotient of captured particles over total particles,
- filter life-time: filtration time until a certain pressure-drop increase is reached,
- filter capacity: mass of particles that can be deposited inside the filter

Many filter media are fibrous in nature and their properties depend on media thickness, fiber diameter, fiber orientation, and pore size distributions.
The permeability, flow resistivity and initial pressure drop can be computed with the EJ, SIMPLE-FFT, or LIR solvers. Based on flow resistivity, even the frequency-dependent acoustic absorption of the fibrous media can be obtained [18]. The filtration process happens in two stages: depth filtration, with particles being deposited inside the filter, and later cake filtration, with particles being deposited on top of the filter (see Fig. 2). The filtration process is simulated by a Lagrangian formulation of particle transport [19]. First, a flow field is computed. Second, particles start from the inlet and move due to their own mass, the friction with the fluid and even Brownian motion, and may be captured on the fibers or on previously deposited particles. These two steps are performed in sequence to ultimately clog the filter. Electrostatic forces can be considered using the negative gradient of a computed potential field [20]. The filter efficiency, life-time, and capacity are obtained as post-processing of a filtration simulation with good agreement compared to measurements [21]. Particle diameters usually span multiple length scales. Particles much larger than a voxel are represented as empty-solid model and particles much smaller than a voxel are modelled by a homogeneous porous media approach [22].

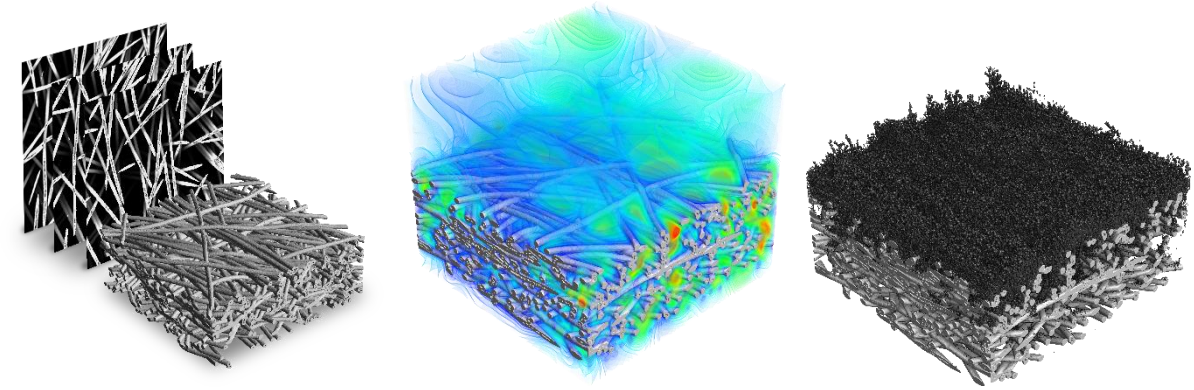

Fig. 2: CT-scan and segmented 3D model of fibrous filter media (left). Stokes flow field through a filter media (center). Captured particles on top and inside of a filter media (right).

3.2 Personal care materials

Many personal care products partly consist of highly porous fiber material. For example, modern diapers are high-tech products consisting of several functional nonwoven and superabsorbent polymer layers. The nonwoven layers must be highly permeable so that fluids can pass through fast and reach the superabsorbent polymer layers. In addition, the permeability changes under mechanical loads.
With the LIR and Explicit Jump methods, absolute permeability is predicted fast and precisely [23]. The pore morphology method allows to predict drainage and imbibition capillary pressure curves that match laboratory measurements. The mechanical deformation of these nonwoven layers is effectively predicted with the Lippmann-Schwinger methods in the FeelMath solver.

3.3 Digital Rock Physics

Digital rock physics (DRP), i.e. the determination of physical rock properties by performing numerical simulations on 3D scans of rock samples, represents an innovative technique that reduces time and cost compared to conventional laboratory experiments. DRP can be used as a complementary technique to these experiments, also serving as a quality assurance tool of the experiments and vice versa. Besides the increase in efficiency, DRP also allows insights into the actual processes taking place in the samples and is considered a game changer for the Oil and Gas industry.
One of the first steps in a simulation workflow is the image acquisition, processing, and segmentation to create a digital rock model [24]. These steps are crucial and must be done very carefully. Researchers and petroleum engineers are often interested in porosity, pore-body and pore-throat size distributions, tortuosity, absolute and relative permeability, electrical conductivity, stiffness, and compression-dependent properties.

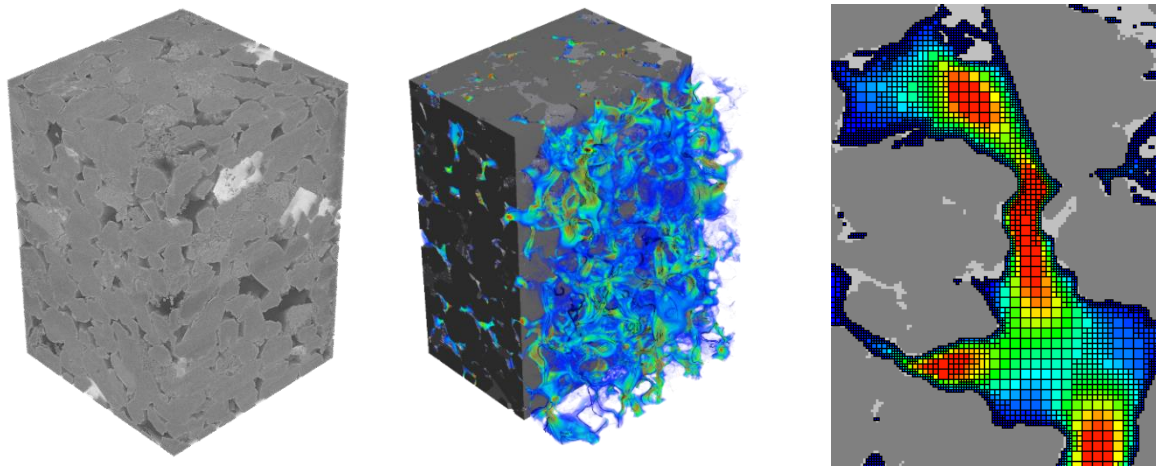

Fig. 3: CT-scan of a Berea sandstone (left). Stokes flow field through a segmented Berea sandstone (center). Adaptive grid visualization of the LIR-Stokes solver (right).

The porosity is often below 20%, pore networks are complex, and flow percolation paths can be narrow. Fig. 3 shows the flow field inside such a complex Berea sandstone. Properties computed by different solvers may deviate up to 50% depending on the discretization, boundary conditions, or stopping criteria

[25]. The EJ, SimpleFFT, and LIR flow solvers show a very good performance in a benchmark study with six other solvers [26]. The adaptive grid of the LIR solver allows to predict permeability on very large rock models with more than 5 billion voxels [27]. Computed capillary pressure curves of the pore morphology method and computed relative permeabilities agree with measurements [28].

3.4 Battery cathode materials

The development of new battery materials and designs has become crucial in recent years. Electromobility is a worldwide growing trend bringing heavy demands on modern batteries. Batteries should have high capacity, low charging time, be safe to use, and sustain a long-life cycle. These requirements are hard to satisfy all at once.
A lithium-ion battery is built with a cathode side and an anode side with a separator between them. The cathode and anode consist of active material that hosts lithium atoms. The active materials are embedded in binder material and carbon black with high electric conductivity. The pore space is filled with electrolyte which is diffusive for lithium ions. During battery charging, lithium atoms leave the active material while losing an electron and turning into lithium ions (Li+). They travel through the electrolyte and the separator, from the cathode to the anode side. The electrons (e-) also travel from the cathode to the anode side but through the binder and the surrounding electric circuit. Then, lithium ions combine with the electrons and the resulting lithium atoms enter the active material on the anode side.
In an ideal battery, the amount of binder and its distribution provides a very high electric conductivity while leaving enough space for the electrolyte with a high diffusivity. The conductivity, diffusivity, and tortuosity are properties predicted using the Explicit Jump or LIR methods [29]. During battery charging, active materials grow on the anode side and shrink on the cathode side. Subsequent internal mechanical stress is predicted using the Lippmann-Schwinger methods [30]. The simulation workflow shown in Fig. 4 has similarities with the DRP workflow.

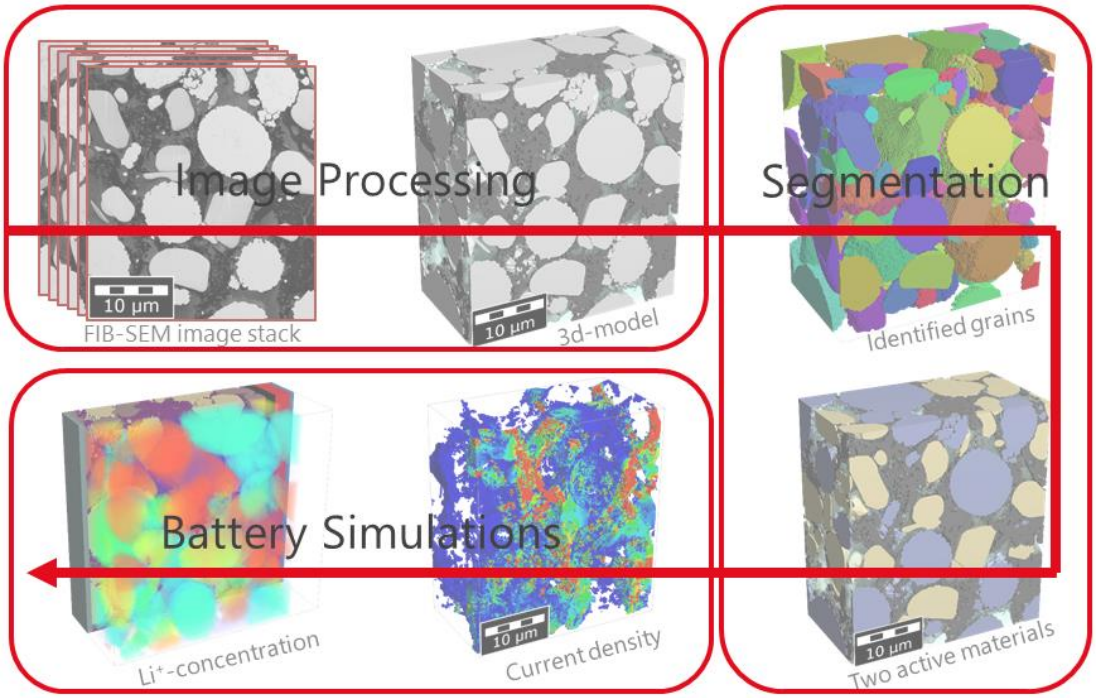

Fig. 4: Workflow for battery simulation starting from image acquisition, image processing, segmentation, and prediction of properties.

3.5 Gas Diffusion Layers (GDL)

Fuel cells are another promising technology used in automotive industry to convert chemical energy into electricity through electrochemical reactions of hydrogen and oxygen. The structure of a fuel cell has similarities to a battery: anode side, a separator, and a cathode side. The GDL is a nonwoven porous structure made of carbon fibers that plays an important role for the transport of reactants and products in the anode and cathode side. Hydrogen comes from the anode side, loses its electron and travels as hydrogen-ion through the separator to the cathode side. The electrons travel through the conducting carbon fiber and the surrounding electric circuit to the cathode side. Hydrogen-ions, electrons and oxygen merge to water and heat at the cathode side.
Important properties of GDL are the distribution of water, capillary pressure, relative permeability of water, gas diffusivity, the electrical and thermal conductivity, and its behavior under mechanical

compression [31]. The EJ and LIR conduction solvers predict the gas diffusivity and electric conductivity whereas the EJ, SIMPLE-FFT, and LIR stokes flow solvers predict the absolute permeability in agreement with measurements for different levels of compression [32]. The fibers of a GDL can be hydrophilic or hydrophobic depending on their coating, e.g. under Teflon treatment. The distribution of water and the capillary pressure curves can be predicted with the pore morphology methods for both cases [33]. The water acts as a barrier to the gas diffusion process. The computed distribution of water allows then to compute relative permeabilities, as well as relative gas diffusivities [34]. Thermal management is also one of the crucial topics in fuel cells, especially in GDL. With the conduction solvers, it is possible to predict thermal conductivity [35].

3.6 Fiber Reinforced Composites

Composite materials and digital material engineering of composites are essential in current component development to improve the functionality and lightweight design in automotive and other industries, and in many industrial applications. The simulation tool's ability to create realistic representative microstructure models and to determine their physical material properties, helps in quicken product development profitably. Lippmann-Schwinger methods and the FeelMath solver are especially suited for this application because they allow a fast and accurate prediction of the full mechanical stiffness tensor, as well as elastic moduli, which agrees with measurements [36]. With non-linear material models it is possible to simulate the evolution of deformation and damage within microstructures [37].

4 Conclusions

The presented numerical methods predict flow, conduction, and mechanical properties with high agreement to experimental measurements. The methods are highly optimized and designed to work directly on 3D images that come from µCT or FIB-SEM devices. Computed physical properties help engineers and researchers to understand natural materials and optimize man-made materials on their way to improve processes or material development.

5 References

[1] Steiner, K. and Ginzburg, I.: "Lattice Boltzmann model for free-surface flow and its application to filling process in casting", Journal of computational physics, 2003 (185), pp. 61-99.

[2] Moulinec, H. and Suquet, P.: "A FFT-Based Numerical Method for Computing the Mechanical Properties of Composites from Images of their Microstructures", IUTAM Symposium on Microstructure-Property Interactions in Composite Materials, 1995 (37), pp. 235-246.

[3] Harlow, F.H. and Welch, J.E.: "Numerical calculation of time-dependent viscous incompressible flow of fluid with a free surface", Physics of Fluid, 1965, pp. 2182-2189.

[4] Wiegmann, A.: "Computation of the permeability of porous materials from their microstructure by FFF-Stokes", Berichte des Fraunhofer ITWM, 2007 (129).

[5] Wiegmann, A. and Bube, K.P.: "The Explicit-Jump immersed interface method: Finite difference methods for PDEs with piecewise smooth solutions", SIAM J. Numer. Anal., 2000 (37)3, pp. 827-862.

[6] Swarztrauber, P. N.:"A direct method for the discrete solution of separable elliptic equations", SIAM J. Numer. Ana., 1974 (11)6, pp. 1136-1150.

[7] Van der Vorst, H. A.: "Bi-CGSTAB: A Fast and Smoothly Converging Variant of Bi-CG for the Solution of Nonsymmetric Linear Systems", SIAM J. Sci. and Stat. Comput., 1992 (13)2, pp. 631–644.

[8] Wiegmann, A. and Zemitis, A.: "EJ-HEAT: A Fast Explicit Jump Harmonic Averaging Solver for the Effective Heat Conductivity of Composite Materials", Berichte des Fraunhofer ITWM, 2006 (94).

[9] Patankar, S.V.: "Numerical heat transfer and fluid flow", Taylor & Francis, 1980, pp. 126-134.

[10] Linden, S. et al.: "The LIR space partitioning system applied to the Stokes equations", Graphical Models, 2015 (82), pp. 58-66.

[11] Linden, S. et al.: "The LIR space partitioning system applied to Cartesian grids", Mathematical methods for curves and surfaces, 2012, pp. 324-340.

[12] Kabel, M. et al.: "Efficient fixed point and Newton-Krylov solvers for FFT-based homogenization of elasticity at large deformations", Computational Mechanics, 2014 (54), pp. 1497-1514.

[13] Schneider, M. et al.: "Computational homogenization of elasticity on a staggered grid", International journal for numerical methods in engineering, 2016 (105)9, pp. 693-720.

[14] Hilpert, M. and Miller, C. T.: "Pore-morphology-based simulation of drainage in totally wetting porous media", Advances in Water Resources, 2001 (24), pp. 243-255.
[15] Silin, D. et al.: "Microtomography and Pore-Scale Modeling of Two-Phase Distribution", Transport in Porous Media, 2011 (86), pp. 495-515.
[16] Ahrenholz, B. et al.: "Prediction of capillary hysteresis in a porous material using lattice-Boltzmann methods and comparison to experimental data and a morphological pore network model", 2008 (31)9, pp. 1151-1173.
[17] Schulz, V. et al.: "Pore-Morphology-Based Simulation of Drainage in Porous Media Featuring a Locally Variable Contact Angle", 2015 (107)1, pp. 13-25.
[18] Schladitz, K. et al.: "Design of acoustic trim based on geometric modeling and flow simulation for non-woven", Computational materials science, 2006 (38), pp. 56-66.
[19] Latz, A. and Wiegmann, A.: "Simulation of fluid particle separation in realistic three-dimensional fiber structures", Filtech Proceedings Europe conference, 2003, pp. 353-360.
[20] Rief, S. et al.: "Research note: computer simulations of air filtration including electric surface charges in 3-dimensional fibrous microstructures", Filtration, 2006 (6)2, pp. 169-172.
[21] Becker, J. et al.: "Improved modeling of filter efficiency in life-time simulations on fibrous filter media", Filtech Proceedings Wiesbaden, 2013.
[22] Becker, J. et al.: "Simulation of cake filtration for polydisperse particles", Chemical Engineering & Technology, 2016 (39)3, pp. 559-566.
[23] Steiner, K. et al.: "Water transport in cellulosic materials", Berichte des Fraunhofer, 2016, p. 32.
[24] Andrä, H. et al.: "Digital rock physics benchmarks Part I: Imaging and segmentation", Computers & Geosciences, 2013 (43), pp. 25-32.
[25] Andrä, H. et al.: "Digital rock physics benchmarks Part II: Computing effective properties", Computers & Geosciences, 2013 (43), pp. 33-43.
[26] Saxena, H. et al.: "References and benchmarks for pore-scale flow simulated using micro-CT images of porous media and digital rocks", Advances in Water Resources, 2017 (109), pp. 211-235.
[27] Menke, H.P. et al.: "4D multi-scale imaging of reactive flow in carbonates: Assessing the impact of heterogeneity on dissolution regimes using streamlines at multiple length scales", Chemical Geology, 2018 (481), pp. 27-37.
[28] Berg, S. et al.: "Connected pathway relative permeability from pore-scale imaging of imbibition", Advances in Water Resources, 2016 (90), pp. 24-35.
[29] Müller. S. et al. "Quantifying Inhomogeneity of Lithium Ion Battery Electrodes and Its Influence on Electrochemical Performance", Journal of the Electrochemical Society, 2018 (165), pp. 339-334.
[30] Lagadec, M.F. et al.: "Designing Polyolefin Separators to Minimize the Impact of Local Compressive Stresses on Lithium Ion Battery Performance", Journal of the Electrochemical Society, 2018 (165), pp. 1829-1836.
[31] Becker, J. et al.: "Numerical Determination of Two-Phase Material Parameters of a Gas Diffusion Layer Using Tomography Images", Journal of Fuel Cell Science and Technology, 2008 (5)(2), pp. 21006-21014.
[32] Becker, J. et. Al.: "Determination of Material Properties of Gas Diffusion Layers: Experiments and Simulations Using Phase Contrast Tomographic Microscopy", Journal of the Electrochemical Society, 2009 (156), pp. 1175-1181.
[33] Schulz, V.P. et al.: "Modeling of Two-phase Behavior in the Gas Diffusion Medium of Polymer Electrolyte Fuel Cells via Full Morphology Approach", Journal of the Electrochemical Society, 2007 (154)4, pp. 8419-8426.
[34] Zamel, N. et al.: "Effect of liquid water on transport properties of the gas diffusion layer of polymer electrolyte membrane fuel cells", International Journal of Hydrogen Energy, 2011 (36), pp. 5466-5478.
[35] Zamel, N. et al.: "Estimating effective thermal conductivity in carbon paper diffusion media", Chemical Engineering Science, 2010 (65)13, pp. 3994-4006.
[36] Sliseris, J. et al.: "Numerical prediction of the stiffness and strength of medium density fiberboards", Mechanics of materials, 2014 (79), pp. 73-84.
[37] Fliegener, S. et al.: "Investigations into the damage mechanisms of glass fiber reinforced polypropylene based on micro specimens and precise models of their microstructure", Composites. Part B: Engineering, 2016 (105)9, pp. 693-720.